EDGEWOOD CHEMICAL BIOLOGICAL CENTER
U.S. ARMY RESEARCH, DEVELOPMENT AND ENGINEERING COMMAND
Aberdeen Proving Ground, MD 21010-5424

ECBC-TR-1338

USING NMR SPECTROSCOPY TO INVESTIGATE THE SOLUTION BEHAVIOR OF NERVE AGENTS AND THEIR BINDING TO ACETYLCHOLINESTERASE

Terry J. Henderson

RESEARCH AND TECHNOLOGY DIRECTORATE

January 2016

Disclaimer

The findings in this report are not to be construed as an official Department of the Army position unless so designated by other authorizing documents.

REPORT DOCUMENTATION PAGE

Form Approved
OMB No. 0704-0188

1. REPORT DATE *(DD-MM-YYYY)*	**2. REPORT TYPE**	**3. DATES COVERED** *(From - To)*
XX-01-2016	Final	Jan – Jun 2015

4. TITLE AND SUBTITLE
Using NMR Spectroscopy to Investigate the Solution Behavior of Nerve Agents and Their Binding to Acetylcholinesterase

5a. CONTRACT NUMBER
CB3889

5b. GRANT NUMBER

5c. PROGRAM ELEMENT NUMBER

6. AUTHOR(S)
Henderson, Terry J.

5d. PROJECT NUMBER

5e. TASK NUMBER

5f. WORK UNIT NUMBER

7. PERFORMING ORGANIZATION NAME(S) AND ADDRESS(ES)
Director, ECBC, ATTN: RDCB-DRB-C, APG, MD 21010-5424

8. PERFORMING ORGANIZATION REPORT NUMBER
ECBC-TR-1338

9. SPONSORING / MONITORING AGENCY NAME(S) AND ADDRESS(ES)
Defense Threat Reduction Agency, 8725 John J. Kingman Road, MSC 6201, Fort Belvoir, VA 22060-6201

10. SPONSOR/MONITOR'S ACRONYM(S)
DTRA

11. SPONSOR/MONITOR'S REPORT NUMBER(S)

12. DISTRIBUTION / AVAILABILITY STATEMENT
Approved for public release; distribution is unlimited.

13. SUPPLEMENTARY NOTES

14. ABSTRACT:
The general theory for investigating the conformational dynamics of nerve agents in solution by measuring transient proton–proton nuclear Overhauser effect (NOE) build-up curves and the use of molecular dynamics simulations for their interpretation are explained. The phenemonon of nuclear magnetic relaxation is also described in some detail as well as how relaxation measurements can be interpreted with mathematical models of molecular motion and statistical distributions of correlation times to derive molecular dynamics information. Finally, examples of transient NOE measurements and their interpretation to determine an ensemble average conformation for VX in aqueous solution are summarized.

15. SUBJECT TERMS
Acetylcholinesterase (AChE) Conformation Molecular dynamics (MD) Nerve agent
Nuclear magnetic relaxation Nuclear Overhauser effect (NOE) Solution behavior

16. SECURITY CLASSIFICATION OF:			**17. LIMITATION OF ABSTRACT**	**18. NUMBER OF PAGES**	**19a. NAME OF RESPONSIBLE PERSON**
a. REPORT	**b. ABSTRACT**	**c. THIS PAGE**			Renu B. Rastogi
U	U	U	UU	30	**19b. TELEPHONE NUMBER** *(include area code)* (410) 436-7545

Blank

PREFACE

The work described in this report was authorized under Defense Threat Reduction Agency contract no. CB3889. The work was started in January 2015 and completed in June 2015.

The use of either trade or manufacturers' names in this report does not constitute an official endorsement of any commercial products. This report may not be cited for purposes of advertisement.

This report has been approved for public release.

Blank

CONTENTS

FIGURES

USING NMR SPECTROSCOPY TO INVESTIGATE THE SOLUTION BEHAVIOR OF NERVE AGENTS AND THEIR BINDING TO ACETYLCHOLINESTERASE

1. INTRODUCTION

Project CB3889 focuses on elucidating both the mechanistic and thermodynamic details of nerve agent–acetylcholinesterase (AChE) interactions. The role of nuclear magnetic resonance (NMR) spectroscopy in this effort is described herein, with special attention given to the study of nerve agent conformational dynamics in solution and its contributions to the interaction with AChE. The utility of using computer simulations for interpreting the NMR results is also described in some detail. And lastly, some preliminary results regarding the conformation of nerve agent VX in aqueous solution are summarized.

2. CONFORMATIONAL ENTROPY

At physiological temperatures, both nerve agents and the AChE enzyme exist as flexible molecules in solution, but for very different reasons. As with most small organic molecules, nerve agents are not dominated by large networks of aromatic, double and triple bonds that prohibit rotations of chemical groups about bonds and "rigidify" molecular conformation. Additionally, nerve agent molecules are much too small to contain a sufficient number of molecule–molecule contacts (e.g., hydrogen bonds) to lock them into a single conformation. In solution, therefore, nerve agent molecules constantly experience rotations about their single bonds, giving rise to an "ensemble" of different molecular conformations. Some rotations result in the movement of only a few atoms, such as the rotation of a methyl or hydroxyl group. Other rotations give rise to motions involving large segments of the nerve agent molecule, such as those about the nitrogen–carbon bond in VX that displace both isopropyl groups simultaneously. Alternatively, globular proteins, such as AChE, are energetically much more complex than small molecules in solution. In their native states, proteins are not able to simultaneously achieve favorable interactions between all of their protein–protein contacts, which leaves some chemical groups free to interact with solvent molecules. The native state, therefore, is a complex collection of protein–protein and protein–solvent contacts in which a significant portion constantly interconverts between the two contact types. This allows "switching" between large numbers of conformations with very similar energies. The native state is very dynamic and, like small molecules, exists as an ensemble of conformations rather than as a single, rigid conformation. This conformational switching is referred to as "protein frustration" (Bryngelson et al., 1995) or simply "frustration" and arises from the inability of a protein to simultaneously achieve favorable interactions between all of its protein–protein contacts in solution. The most conformationally flexible or frustrated regions of proteins tend to be enzyme-active sites and other sites where naturally occurring ligands bind the protein (Ferreiro et al., 2011). In the past, the conformational dynamics associated with protein frustration was commonly referred to as "protein breathing."

In aqueous solution, the collection of all conformational motions undertaken by both a nerve agent and an AChE enzyme represent all of the conformational changes available to them for their interaction and complexation with each other. To understand these two processes

in a rigorous mechanistic or thermodynamic sense, the small subset of conformational changes explicitly involved must be identified and understood in detail. It is this small set of motions that (a) directly defines the exact mechanism of the nerve agent–AChE interaction, and (b) contributes directly and substantially to the thermodynamic entropy of the interaction. The latter point highlights why these and other conformational motions are commonly referred to as "conformational entropy" by physical chemists and biophysicists. Others refer to these motions as internal motions, conformational dynamics, or sometimes solution behavior. This conformational entropy contributes directly to the change in entropy, ΔS, found in the familiar expression for the Gibbs free energy, $\Delta G = \Delta H + T\Delta S$; where ΔG is the change in Gibbs free energy, ΔH is the change in enthalpy, and T is temperature. The ΔS associated with nerve agent–AChE interactions, therefore, can be investigated by determining the conformational entropy (the solution behavior) of both the nerve agent and the AChE enzyme when they are free in solution, and comparing the entropy to those of the conformations adopted by the two molecules following their complexation. This is the chief reason for using NMR spectroscopy to evaluate the conformational entropy of nerve agents in solution and having a larger, more complex NMR effort to evaluate the solution behavior of free AChE.

The influence of the AChE enzyme on nerve agent solution conformation during the binding process also needs to be identified to understand the process in mechanistic and thermodynamic terms. Although rigid lock-and-key binding has been reported in some antibody–antigen interactions (Amit et al., 1986), the most-common motif for enzymes and antibodies alike appears to be that changes in ligand or substrate conformation accompany binding (for an example, see Glaudemans et al., 1990). It has become widely accepted that proteins induce conformational changes on their ligands and substrates upon binding, thereby selecting a single ligand or substrate conformation from the many that exist in solution. This "induced-fit binding" has certain thermodynamic consequences compared with lock-and-key binding. First, although the existence of a lock-and-key scheme suggests that proteins bind in a low-energy (and thus highly populated) conformation for a ligand or substrate, there is no reason to assume that such a conformation is necessarily bound in an induced-fit scheme, or even that a ligand or substrate has a single, preferred conformation. Second, some portion of the ΔG that is released upon ligand or substrate binding will be used to induce the conformational changes upon the ligand or substrate, which implies that the overall affinity constant will be smaller. These consequences are especially relevant to nerve agent–AChE interactions because of the conformationally flexible nature of nerve agents in solution (Lushington et al., 2010).

Finally, our current understanding of the conformational behavior of nerve agents and the AChE enzyme in aqueous solution can be considered speculative because it derives almost exclusively from computer simulations (see Lushington et al., 2010, for an example) and not from experimental measurements; such measurements are very difficult to find in the scientific literature. The NMR effort in this project will provide the first experimental measurements on nerve agents and the AChE enzyme that can directly provide information on their aqueous solution behavior. These measurements will also be used to guide the development of computer simulations of nerve agent and AChE behavior when free in aqueous solution. This will constitute the first milestone in the construction of computer simulations that accurately represent the various nerve agent–AChE binding processes.

3. TIME SCALES FOR MOLECULAR MOTIONS AND NMR SPECTROSCOPY

There are two types of molecular motions that directly influence NMR signals: overall molecular reorientation, which is more commonly referred to as rotational diffusion or molecular tumbling, and conformational motions. As shown in Figure 1, many conformational motions occur on the nanosecond (ns) timescale, including those described in Section 2 for dilute solutions of nerve agents and proteins such as AChE. The slower conformational motions (on time scales >1 ns) are primarily those encountered by large chemical groups (branches) in high molecular weight polymers (referred to as "segmental motions") or by molecules in either very viscous solutions or in the solid state. The figure also reveals that these nanosecond motions correlate to oscillations at megahertz (MHz) frequencies, a correlation that can be demonstrated mathematically. Any motion occurring over a 2 ns time frame, for instance, can be shown to correspond directly to a 500 MHz oscillation simply by recognizing that 500 MHz and 2 ns are reciprocals of each other. In a similar manner, it can also be shown that motions occurring over a 1 ns or 1 μs time frame correspond to 1 GHz or 1 MHz oscillations, respectively, as shown in Figure 1. The translational diffusion of molecules through three-dimensional space does not influence NMR signals unless magnetic field strength gradients are used when acquiring the NMR signals. This phenomenon allows the measurement of molecular diffusion rates by using NMR experiments that incorporate pulsed-field gradients along one axis within the sample volume.

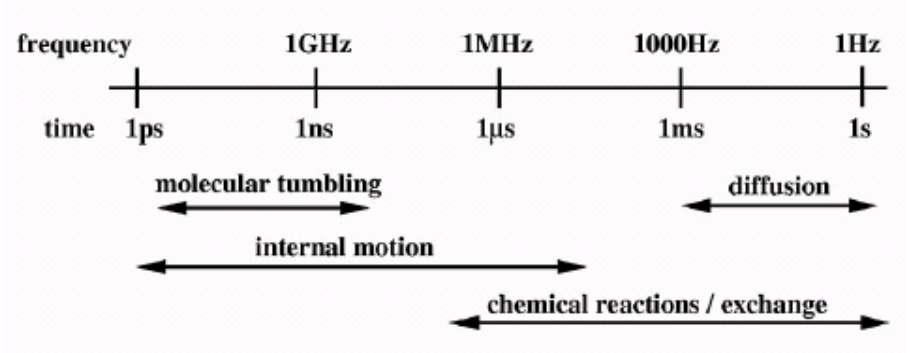

Figure 1. Timescales for high-resolution NMR spectroscopy. Motions occurring on second (s), millisecond (ms), microsecond (μs), nanosecond (ns), and picosecond (ps) timescales are represented with their corresponding oscillation frequencies in hertz (Hz), megahertz (MHz), and gigahertz (GHz). Timescales for overall molecular rotational reorientation (molecular tumbling), molecular translational diffusion (diffusion), conformational dynamics (internal motion), and chemical reactions and exchange events (chemical reactions/exchange) are shown with double-headed arrows.

4. THE NUCLEAR MAGNETIC DIPOLE MOMENT

Subatomic particles (electrons, protons and neutrons) can be imagined as spinning on their axes. In the nucleus of many atoms (e.g., ^{12}C), these spins are paired against each other, and the nucleus has no overall spin. The nuclei of other atoms (including protons and ^{13}C), on the

other hand, are structured in a manner that gives rise to overall spin, or intrinsic angular momentum. These nuclei are composed of an odd number of protons and/or neutrons, and their spin is described by the spin quantum number *I*. As shown in Figure 2a, all nuclei with nonzero spin have a magnetic dipole moment, or magnetic moment (designated as μ), that can be described as a vector quantity having both magnitude and direction. Quantum mechanics states that any nucleus with spin *I* has $2I + 1$ possible orientations, but in the absence of an external magnetic field, these orientations are of equal energy. This degeneracy disappears in the presence of an applied magnetic field, and each orientation assumes a unique energy level that can be given a magnetic quantum number *m*; see Figure 2b.

Both the angular momentum and magnetic moment of an NMR-active nucleus define its behavior in a magnetic field, as well as the consequences of molecular motions on NMR signals. For example, the gyromagnetic ratio (ratio of a particle's magnetic moment to its angular momentum) for protons dictate that their magnetic moments will precess (spin) at 500 MHz in a static magnetic field of 11.75 T (Tesla), and that oscillations at this same frequency can cause transitions between the two proton spin states (Figure 2b). This oscillating field can be provided by either (a) a 500 MHz radio frequency pulse or (b) molecular motions occurring over a 2 ns timescale. In NMR spectroscopy, radio frequency pulses are used to perturb the steady-state system established between NMR-active nuclei and a static magnetic field so that NMR signals can be acquired. Molecular motions can then drive transitions between the spin states that return the perturbed system back to its steady-state condition, a process referred to as "nuclear magnetic relaxation". It is this intimate relationship between nuclear magnetic relaxation and molecular motion that gives NMR spectroscopy its tremendous utility for investigating molecular dynamics (MD).

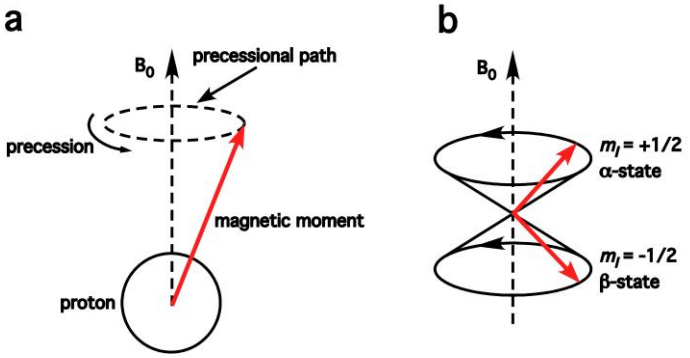

Figure 2. Nuclear magnetic moments and precession. The magnetic moment (red) of a proton ($I = {}^1/_2$) precessing in an applied magnetic field (B_0), and the two precessional cones resulting from the proton's two spin states ($m_I = +{}^1/_2$ and $m_I = -{}^1/_2$) are illustrated in panels a and b, respectively. The circular path of precession is the result of the magnetic moment interacting with the magnetic field. The precession frequency is directly proportional to the magnetic field strength. The spin states $m_I = +{}^1/_2$ and $m_I = -{}^1/_2$ can be referred to as the α- and β-states, respectively.

5. NUCLEAR MAGNETIC RELAXATION AND MD

The most-common approach for using nuclear magnetic relaxation to investigate molecular motions is to measure the relaxation processes for individual NMR signals following a radiofrequency pulse before interpreting them with mathematical models that describe explicit molecular motions. This relaxation and the use of models of molecular motion for interpreting their measurements are described separately. Another type of relaxation referred to as cross-relaxation is also described in this section. Cross-relaxation gives rise to the nuclear Overhauser effect (NOE) and the ability to derive conformational information from NMR spectroscopy.

5.1 Spin–Lattice and Spin–Spin Relaxation Times

Nuclear magnetic relaxation processes are very complex phenomena that encompass a great number of individual processes; however, they can almost always be modeled as single-exponential events occurring over microseconds, milliseconds, or seconds. The most widely used parameters for describing relaxation are the spin–lattice and spin–spin relaxation times designated as T_1 and T_2, respectively. T_1 describes the buildup of bulk magnetization (vector sum of all magnetic moments in a sample) along the direction of the static magnetic field (assigned as the *z* axis by convention) after a perturbation of the steady-state condition, such as that resulting from the application of a radio-frequency pulse for signal measurement. T_2 describes the decay of bulk magnetization in a plane perpendicular to the static magnetic field (the *x*–*y* plane) following the use of a radio frequency pulse to reorient the bulk magnetization into the plane. The bulk magnetization gives rise to the NMR signal, and the progression of spin–lattice or spin–spin relaxation is easily monitored by measuring the intensity of the signal over time. Figure 3 shows the progression of spin–lattice and spin–spin relaxation for a hypothetical NMR signal, which reveals the exponential nature of the two processes.

T_1 and T_2 values change appreciably with the time frame over which molecular motions occur. T_2 values, for instance, increase directly with temperature as all molecular motion is accelerated at increased temperatures. The same set of molecular motions occur at higher temperatures but over shorter time frames. The relationship of spin–lattice relaxation with molecular motion time frame is more complex, with T_1 values either increasing or decreasing with temperature. For low molecular weight molecules, such as nerve agents, T_1 values increase directly with temperature. Conversely, T_1 values decrease for large molecules like proteins with increases in temperature. Because molecular tumbling rates decrease with increasing molecular size, molecular weight can have an appreciable influence in T_1 and T_2 values, and the same molecular motions occurring over the same time frame can give different T_1 values at different magnetic field strengths. Together with the molecular tumbling, the unique combination of all internal motions encountered at one atomic site of a molecule in solution will result in a unique set of T_1 and T_2 values at a specific temperature and magnetic field strength.

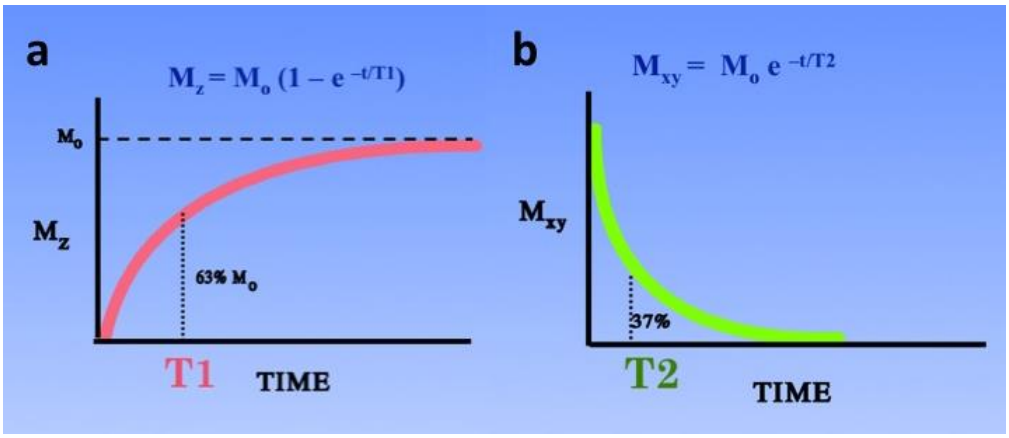

Figure 3. Spin–lattice and spin–spin relaxation. Panel a illustrates the progression of spin–lattice relaxation for a hypothetical NMR signal after reorientation of the bulk magnetization (M_z) in a direction opposite to that of the static magnetic field. Panel b shows the progression of spin–spin relaxation for the signal after reorientation of the bulk magnetization into a plane perpendicular to the static field (M_{xy}). Reorientation in both cases is achieved by the application of appropriate radio frequency pulses. The single exponential equations in each panel describe the progression of relaxation in that panel. The figure includes the terms for bulk magnetization, aligned with the static magnetic field before reorientation (M_0), time (t), and the spin–lattice (T_1) and spin–spin (T_2) relaxation times. T_1 represents the time required for M_z to grow from 0 to 63% of its final value after reorientation of the bulk magnetization, and T_2 represents the time required for M_{xy} to decay to 37% of its initial maximum value after this reorientation.

5.2 The NOE

The NOE represents a special case of relaxation because it only occurs when the spin states for one nucleus are saturated (the populations of the α- and β-states in Figure 2b are manipulated to become equal and are designated mathematically as $N_\alpha = N_\beta$). This is easily accomplished by decoupling techniques which are the same as those used to generate proton-decoupled NMR spectra. A second requirement for the NOE is that two or more NMR-active nuclei must be sufficiently close to one another to allow dipolar coupling, defined as the direct interaction between their two magnetic diploes. As shown in Figure 4, all nuclear magnetic moments have an associated magnetic dipole with a magnetic field, which are both oriented in a direction parallel to that of the nuclear spin vector. Two NMR-active nuclei in close enough proximity to each other will have overlapping magnetic fields (Figure 4c), resulting in the coupling of their magnetic dipoles. The strength of this dipole–dipole interaction depends strongly on the distance separating the two nuclei as well as their gyromagnetic ratios. Under these conditions, saturating the spin states of one nucleus will result directly in the enhancement of the NMR signal of the other nucleus.

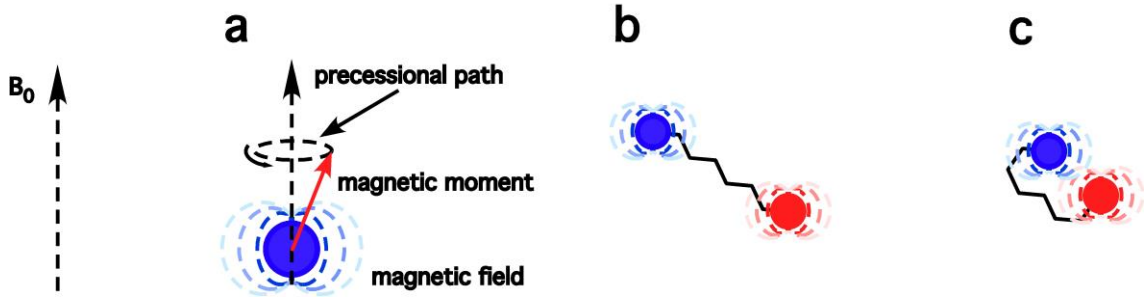

Figure 4. Dipolar coupling. Panel a shows the magnetic field associated with the magnetic dipole of an NMR-active nucleus together with its magnetic moment. Panels b and c show two NMR-active nuclei of the same molecule in a magnetic field (B_0). The nuclei are not close enough in conformational space to be dipolar-coupled in panel b, but the conformational change shown in panel c brings them close enough to become dipolar-coupled. The magnetic fields for the red and blue nuclei are illustrated with magnetic field lines (red and blue dashed lines, respectively). The colors of the field lines become progressively lighter with an increase in distance from the nuclear center to represent the decrease in magnetic field strength.

The origin and effects of the NOE on NMR signals are most easily described in terms of a system of two identical NMR-active nuclei (referred to as a homonuclear two-spin system) of spin $^1/_2$ ($I = {}^1/_2$). When the spins are dipolar-coupled, their four energy states can be diagrammed as shown in Figure 5. By convention, the spins are designated *I* and *S*, where, *I* is the spin whose resonance (or NMR signal) is being measured, and *S* is the spin whose resonance is being saturated in a NOE experiment. For simplicity, it can be assumed that the two spins are both in the same conformationally rigid molecule, are not scalar-coupled ($J_{IS} = 0$), and that their dipole–dipole interaction dominates nuclear magnetic relaxation. The spin states of the two nuclei are represented in the diagram, and the transitions between them are designated by the conventional nomenclature for their corresponding probabilities (W_{1I}, W_{1S}, W_{0IS}, and W_{2IS}).

Transitions around the perimeter of the energy diagram (the two W_{1I} transitions and two W_{1S} transitions) are all single-quantum transitions that exist even when the two nuclei are far apart from one another and are not dipolar-coupled. These are single-spin transitions (involving only one nucleus) and give rise to signals in NMR spectra. The chemical shifts of the signals in NMR spectra are direct reflections of the energy differences between the two states involved in the transitions. The remaining two transitions, those labeled as W_{0IS} and W_{2IS}, involve the simultaneous "flip" of both spins ($\alpha\alpha \leftrightarrow \beta\beta$ and $\alpha\beta \leftrightarrow \beta\alpha$) and can only occur in dipolar-coupled nuclei. These two-spin transitions have no analogy in single-spin systems and are central to the NOE phenomenon because they give rise to NOE enhancements by allowing saturation of the *S* nucleus to affect the signal intensity of the *I* nucleus. Although they are forbidden transitions in the conventional sense, which means they cannot be directly excited by a radio frequency pulse or give rise to NMR signals in spectra, they are not forbidden in the context of nuclear magnetic relaxation. The $\alpha\alpha \leftrightarrow \beta\beta$ transition is referred to as the double-quantum, double-flip, or W_2 transition because its energy difference corresponds to that of two single-quantum transitions (W_{1I} and W_{1S}). In contrast, the $\alpha\beta \leftrightarrow \beta\alpha$ transition is referred to as the zero-quantum, flip-flop, or W_0

transition because its energy difference corresponds to a net zero quantum change. Collectively, the transitions are known as the cross-relaxation pathways, or simply cross-relaxation.

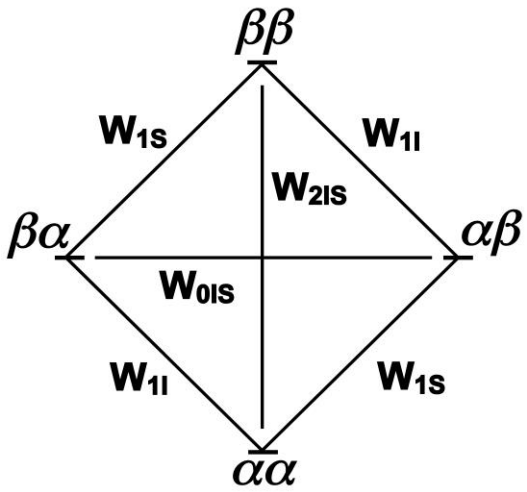

Figure 5. Energy level diagram for a system of two dipolar-coupled, $^1/_2$-spin nuclei. The diagram shows the definitions for single-quantum transition probabilities (W_{1I}, W_{1S}), the zero-quantum transition probability (W_{0IS}), and the double-quantum transition probability (W_{2IS}), as well as all spin states (α and β, as shown in Figure 2b) of a system of two dipolar-coupled, $^1/_2$-spin nuclei. The spin states are designated with the measured nucleus (I) first followed by that of the saturated nucleus (S). For example, $\alpha\beta$ indicates that the measured nucleus is in the α-state and the saturated nucleus in the β-state.

Figure 5 can also be used to discuss how cross-relaxation causes NOE enhancements. The NOE enhancement $f_I\{S\}$ is defined as the fractional change in the signal intensity of nucleus I upon saturating nucleus S

$$f_I\{S\} = (I - I^0)/I^0$$

where I^0 is the signal intensity of nucleus I under steady-state conditions (such as before the application of a radio frequency pulse to acquire a signal). The diagram reveals that the signal intensity of nucleus I is proportional to the sum of the two population differences represented by the W_{1I} transitions for the nucleus, or $(N_{\alpha\alpha} - N_{\beta\alpha}) + (N_{\alpha\beta} - N_{\beta\beta})$. The signal intensity of the S nucleus is proportional to the sum of the two population differences represented by the W_{1S} transitions, or $(N_{\alpha\alpha} - N_{\alpha\beta}) + (N_{\beta\alpha} - N_{\beta\beta})$. For a homonuclear system under steady-state conditions, level αα is populated the most, followed by αβ and βα with populations that are essentially identical to one another, and followed in turn by level ββ.

The consequences of saturating the spin states of one nucleus in a system of two dipolar-coupled, $^1/_2$-spin nuclei are detailed in Figure 6. The figure starts with steady-state conditions (Figure 6a), where the same population difference exists across all four single-quantum transitions ($\alpha\alpha \leftrightarrow \beta\alpha$, $\alpha\alpha \leftrightarrow \alpha\beta$, $\alpha\beta \leftrightarrow \beta\beta$, and $\beta\alpha \leftrightarrow \beta\beta$) so that the equilibrium signal intensities for nuclei *I* and *S* are identical. Saturation of the spin states of nucleus *S* equalizes the population levels $\alpha\alpha$ and $\alpha\beta$ and similarly equalizes those of $\beta\alpha$ and $\beta\beta$, which therefore increases the population levels of $\alpha\beta$ and $\beta\beta$ while decreasing the population levels of $\alpha\alpha$ and $\beta\alpha$ (Figure 6b). There is no immediate change in the signal intensity of the *I* nucleus because the population differences ($N_{\alpha\alpha} - N_{\beta\alpha}$) and ($N_{\alpha\beta} - N_{\beta\beta}$) are unchanged at this point. However, several relaxation and cross-relaxation processes can occur moving forward from this point.

The W_{1I} and W_{1S} transitions can produce spin–lattice relaxation of nuclei *I* and *S*, respectively, with each relaxation process occurring independently of the other. However, the double-quantum transition (W_{2IS} in Figure 5) can also occur and will act to restore the populations of the $\alpha\alpha$ and $\beta\beta$ levels toward their steady-state equilibrium values (Figure 6c). Saturation of the spin states of nucleus *S* caused the population of level $\beta\beta$ to increase and that of $\alpha\alpha$ to decrease. Therefore, the W_2 relaxation will act to reverse this, which leads to a decrease in the population of the $\beta\beta$ level and an increase in the population in the $\alpha\alpha$ level. This necessarily results in an increase in the population differences ($N_{\alpha\alpha} - N_{\beta\alpha}$) and ($N_{\alpha\beta} - N_{\beta\beta}$) or, in other words, an increase in the signal intensity of nucleus *I*. Thus, if a W_2 transition occurs, it produces a positive NOE enhancement in the NMR signal of nucleus *I*.

Another cross-relaxation process that can occur after saturation of the spin states of nucleus *S* is the zero-quantum transition (W_{0IS} in Figure 5). By using an analogous argument, it can be shown that upon saturating the spin states of the *S* nucleus, zero-quantum relaxation across the W_0 transition can lead to a decrease in the signal intensity of nucleus *I* and a negative NOE enhancement (Figure 6d). The NOE is not an instantaneous phenomenon but usually builds up over a time frame of hundreds of milliseconds to seconds. The proton–proton NOE is usually measured during the early part of this buildup to extract proton–proton distances for determining the conformation of molecules, which includes the three-dimensional structure of proteins (Section 6.0). For investigating MD with models of molecular motion, proton–^{13}C NOE enhancements are most often measured under conditions of continuous saturation of the proton spin states late in the build-up process when steady-state conditions have been reached. Because proton–^{13}C bond lengths are very similar from one bond to the next, the proton–^{13}C steady-state NOE values measured in NMR experiments are exclusively the result of molecular motions. In an analogous approach, the proton–^{15}N steady-state NOE is used to study the backbone dynamics of proteins (Ferrage et al., 2008).

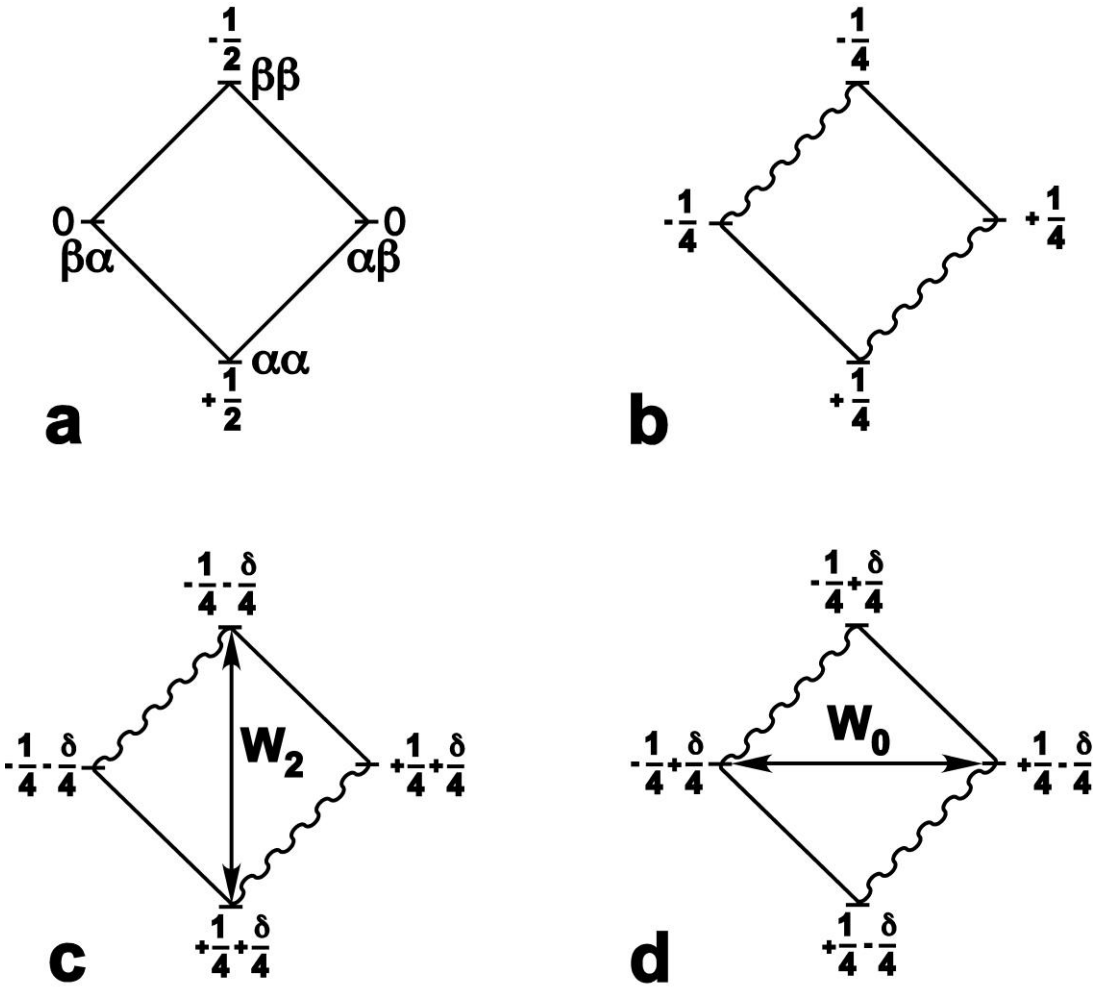

Figure 6. Origin of the NOE in a homonuclear system of two dipolar-coupled, $^1/_2$-spin nuclei. The signal intensity I_0 (where $I_0 = S_0$) is represented by a total spin population difference of one unit, and, for convenience, the spin populations $N_{\alpha\beta}$ and $N_{\beta\alpha}$ are set to zero. Panel a represents the steady-state situation at thermal equilibrium, and panel b represents the situation after saturation of the spin states of nucleus *S*. In panel b, the $N_{\alpha\alpha}$ and $N_{\alpha\beta}$ spin populations are equalized after saturation, as are $N_{\beta\alpha}$ and $N_{\beta\beta}$. The signal intensity of nucleus *I* is still one unit, but that of nucleus *S* is now zero because the equal spin populations from saturation cancels each other's contribution to generating a NMR signal. Panel c shows the effect of W_2 relaxation during the saturation of the spin states of nucleus *S*. Spin population ($\delta/2$ units) has been transferred from the $\beta\beta$ state to the $\alpha\alpha$ state, and saturation of the spin states of nucleus *S* maintains the population equality across the W_{1S} transitions. This increases the signal intensity of nucleus *I* to $(1 + \delta)$ units, which generates a positive NOE enhancement. Panel d shows the effect of W_0 relaxation during the saturation of the spin states of nucleus *S*. Spin population ($\delta/2$ units) transfers from the $\alpha\beta$ state to the $\beta\alpha$ state, which changes their spin populations in the direction of equilibrium. This decreases the signal intensity of nucleus *I* to $(1 - \delta)$ units and generates a negative NOE enhancement. (See Figure 5 for all transition and spin-state labels.)

5.3 Models of Molecular Motion and Distributions of Correlation Times

T_1, T_2, and steady-state NOE values can yield valuable insight into the relaxation processes that occur at specific atomic sites within a molecule. To extend this insight, efforts can include evaluating different mathematical models of molecular motion for their abilities to reproduce T_1, T_2, and NOE measurements that were observed for one or more atomic sites in a molecule; examples of such models are illustrated in Figure 7. The models usually contain at least one rotational correlation time describing molecular tumbling. In Figure 7, for example, τ_c is used to describe molecular tumbling for highly symmetrical molecules, such as methane or fullerines (buckeyballs), where rotation about all three axes describing the molecule's tumbling in three-dimensional space is equal because of symmetry (all three orthogonal rotations have equal inertia). τ_x and τ_z (Figure 7) describe molecular tumbling for molecules with two rotational axes related by symmetry (two rotational axes have equal inertia and the third axis has a unique inertia), including all cylindrical-shaped molecules (e.g., double-stranded DNA fragments or peptide α-helices) or frisbee-shaped molecules such as benzene. Some models contain additional correlation times for describing conformational motions such as τ_e in Figure 7.

Distributions of correlation times are not mathematical models; they are statistical distributions of large numbers of correlation times used for describing the countless internal motions encountered by a single atomic site within a random coil molecule in solution. Typically, the models or distributions are least-squares fit to a set of measured T_1, T_2, and NOE values by adjusting their characteristic correlation times to identify those that best reproduce the observed values. Often, models and distributions are evaluated by starting with the simplest of these and working progressively towards more-complex models or distributions until one accurately reproduces the observed relaxation times and NOE enhancements. Data sets can include relaxation time and NOE data that are measured at different magnetic field strengths, which allow for more-rigorous and discriminating model evaluation. The interpretation of relaxation data with models of molecular motion provides information about the motional frequencies involved in molecular tumbling and internal motion processes. Alternatively, using distributions of correlation times can provide information about the dynamic range of motional frequencies encountered by random coil molecules.

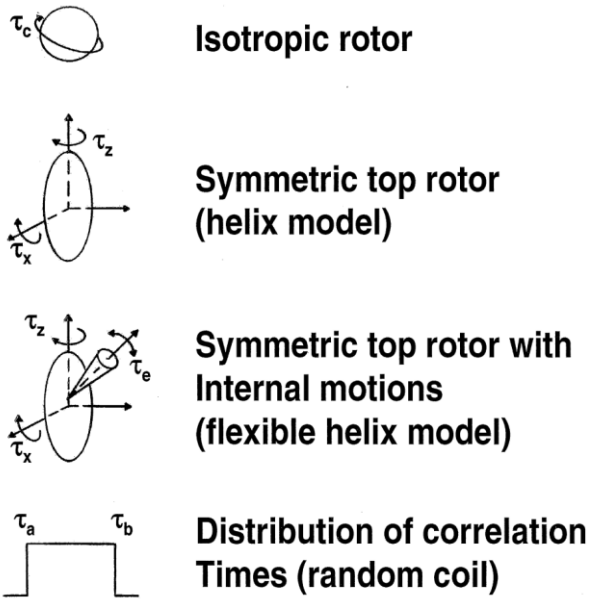

Figure 7. Example models of molecular motion and a distribution of correlation times. τ_c is the correlation time for the molecular tumbling of a rigid sphere. τ_x and τ_z are the correlation times for a rigid ellipsoid about its minor (*x*) and major (*z*) axes, respectively. The latter model is typically used for molecular helices such as small fragments of DNA. The symmetric top rotor with internal motions superimposes an effective correlation time, τ_e, onto a symmetric top rotor to account for internal motion. τ_a and τ_b are the upper and lower bounds, respectively, of a rectangular distribution of correlation times that are used to represent the many dynamic processes in very flexible molecules, which are often referred to as "random coil molecules".

6. THE TRANSIENT NOE AND NOE BUILD-UP CURVES

Using models of molecular motion to interpret NMR data can reveal regions of a molecule that are conformationally dynamic and those that are rigid and ordered. However, these interpretations alone cannot provide any conformational information associated with the solution behavior of molecules or molecular interactions such as nerve agent–AChE binding. Fortunately, such information can be derived directly from the measurement of NOE enhancements because the NOE results from an interaction between nuclei through conformational space. The enhancements most often measured for deriving conformational information are transient NOE enhancements between two dipolar-coupled protons within the same molecule. Figure 8 shows several example build-up curves for such transient NOE enhancements. The earliest events of the build-up curves are the most important for measuring proton–proton distances (and, therefore, conformational information) because these events are exclusively governed by cross-relaxation processes (W_0 and W_2 in Figures 5 and 6). The proton–proton NOE builds up over time (usually hundreds of milliseconds) at a rate inversely proportional to the distance separating the protons raised to the sixth-power (build-up rate $\propto r^{-6}$). This sixth-power dependence dictates that a small change in the proton–proton distance results in a large change in the build-up rate, which makes the use of transient NOE enhancements very accurate for measuring distances between any two

dipolar-coupled protons. Proton–proton distances extracted from NOE data are used almost exclusively in structural and conformational determinations of molecules in solution. In the case of ordered, rigid molecules, this distance information can be the used to directly determine the three-dimensional structure of the molecule. For flexible molecules, on the other hand, the information can give the ensemble-averaged conformation (the weighted-average of all existing conformations) for the molecule in solution. Although determining ensemble-averaged conformations from NOE data is usually straightforward, unraveling their individual, contributing conformations can present a challenge. Project CB3889 will use MD simulations and other computational methods to identify the individual nerve agent conformations contributing to their ensemble-averaged solution conformations determined from NOE data.

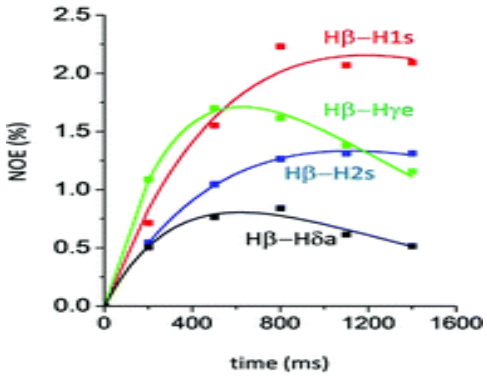

Figure 8. Examples of NOE build-up curves for different proton pairs. The percent NOE buildup is shown as a function of time in milliseconds. The Hβ and Hγe protons (green) are the closest two protons represented in the figure, and they exhibit the fastest build-up rate. The Hβ and Hδa protons (black) are separated by the most distance out of all protons represented in the figure and display the slowest build-up rate. The small decays observed at the later parts of the build-up curves are due to spin–lattice relaxation at both the *I* and *S* nuclei. In the figure, transient NOE enhancements would be measured somewhere between 100 and 300 ms for deriving proton–proton distances.

7. MD SIMULATIONS AND NERVE AGENT–ACHE INTERACTIONS

In the simplest of terms, MD simulations are computer-generated animations of the physical motions of atoms and molecules in conformational space that are calculated directly from numerical methods. The atoms and molecules are allowed to interact for a given period of time to create a visual representation of the atoms in motion, and therefore, of conformational dynamics. Much of our understanding of AChE conformational dynamics was derived from MD simulations, and almost all of the simulations have focused sharply on the AChE active site for studying the catalytic deacylation mechanism of acetylcholine (Lushington et al., 2010). Other AChE-based simulations have focused on the enzyme's interaction with the snake toxin fasciculin (Radic et al., 1995) and a number of dementia drugs (see Cavalli et al., 2004 for an example, or Lushington

et al., 2010 for a review), as well as the actions of covalent inhibitors on the enzyme such as the nerve agent soman (Enyedy et al., 2001). In each case, there were no experimental investigations used to evaluate whether the simulations realistically represented the ligand–AChE interaction investigated. A central tenant of project CB3889 is to provide NMR data deriving directly from the conformational dynamics under investigation for use in developing their MD simulations. The approach centers on consistently improving and refining the initial MD simulations created from estimated parameters for G- and V-series nerve agents and other organophosphorus compounds. The refinement process is based on comparing the transient NOE build-up curves measured for the nerve agents free in solution (Section 5.0) to those calculated directly from the MD simulations under development. Refined simulations should faithfully reproduce the NOE build-up curves, which were measured for the nerve agents at the same temperature and pressure. During the course of a simulation, transient NOE build-up curves will be calculated using r^{-6} averaging ($\langle r^{-6} \rangle$), where r is the proton–proton distance measured from the MD trajectory files that contain the atomic coordinates for the nerve agent conformations. The refined simulations will be used to derive the mechanistic and thermodynamic information for nerve agent–AChE interactions (Sections 7.1–7.3). A related effort later in the project will concentrate on determining nerve agent conformations in their complexes with the AChE enzyme.

7.1 Determination of Nerve Agent Conformational Preferences in Solution

Proton–proton distances and other conformational constraints will be evaluated for nerve agents in solution by the analysis of vicinal proton–proton coupling constants (J_{HH}) and transient NOE build-up curves. Restrained MD calculations of the nerve agents in a vacuum and in water will be conducted to determine which conformations are compatible with the NOE data. Nerve agent flexibility may also be examined through the analysis of relaxation time data, analysis of the NOE data, and molecular modeling. This task will (a) determine the solution conformational preferences and (b) simulate the initial conformational entropy of each nerve agent investigated, which will reflect the state of the agent before AChE interaction.

7.2 Analysis of Changes in Nerve Agent Conformation and Its Associated Thermodynamics

For each nerve agent investigated, the deduced conformational preference in solution, as well as the bound conformation determined from the NOE data and X-ray crystallography, will be used to evaluate the conformational changes associated with AChE interaction. Refined MD simulations will be used to calculate the change in energy for the nerve agent upon binding. This will allow a more detailed understanding of (a) the conformational induction process and (b) the overall associated changes in entropy, enthalpy, and free energy. This particular task can answer questions such as whether AChE binds a low energy (i.e., highly populated) conformation of the nerve agent, and whether some portion of the free energy released upon binding is used to induce nerve agent conformational changes.

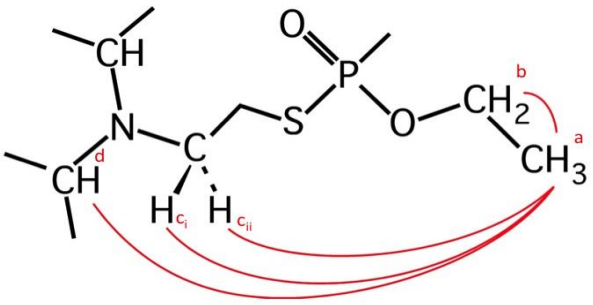

Figure 9. Dipolar-coupled proton pairs in VX. The four dipolar-coupled proton pairs (red lines) identified in this effort for aqueous VX were (1) the H_a–H_b pair, (2) the H_a–H_{ci} pair, (3) the H_a–H_{cii} pair, and (4) the H_a–H_d pair.

7.3 Transient NOE Measurements for VX

This section describes the progress in the identification and measurement of transient NOE enhancements for different proton pairs of VX in aqueous solution at the time of this report. As shown in Figure 9, a total of four dipolar-coupled proton pairs were identified at 600 MHz (14.12 T) and 25 °C. Three of these pairs are long-range dipolar couplings that involve protons located at different ends of the VX molecule. Because dipolar-coupled protons are likely to be separated by <5 Å, the long-range pairs suggest that the ensemble-averaged conformation for aqueous VX is one where the molecule is folded upon itself to bring the *O*-ethyl group and at least one of the *N*-isopropyl groups into close proximity to one another. The transient NOE buildup for each of the four pairs was measured under the same conditions of magnetic field strength and temperature; sample data are shown in Figure 10. Signals for the H_{ci} and H_{cii} protons overlap each other in the spectra, and the build-up curves for the H_a–H_{ci} pair and the H_a–H_{cii} pair were reported as a single, total buildup rather than as two individual curves (Figure 10a). Two such composite curves were measured for these pairs, one from the saturation of the H_c spin states and the measurement of the H_a signal, and vice versa. Together, the curves illustrate that two dipolar-coupled homonuclei display the same build-up kinetics, regardless of which nucleus has its spin states saturated and which has its signal recorded in a NOE experiment.

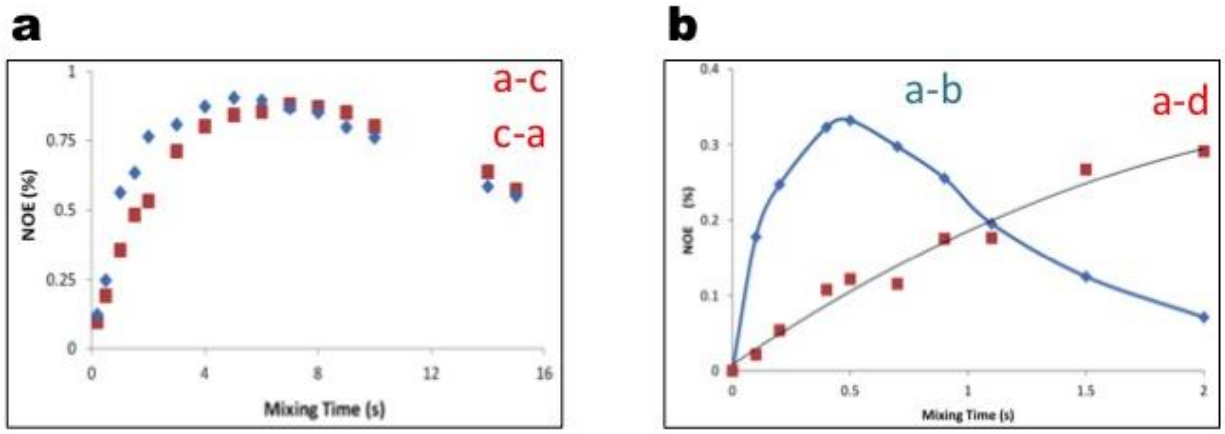

Figure 10. Typical transient NOE build-up curves for proton pairs of aqueous VX. NOE buildup was measured at 600 MHZ and 25 °C for the proton pairs shown in Figure 9. The H_a–H_{ci} and H_a–H_{cii} pairs were combined and reported as single, total buildup (see Section 7.3). Proton pairs are labeled with the measured nucleus first followed by that of the saturated nucleus (a, b, c, and d on each curve set are described in Figure 9).

The NOE data in Figure 10 were used to derive proton–proton distances for determining the ensemble-averaged conformation of aqueous VX. The distances were calibrated against the NOE build-up rate measured for the two aromatic protons of tyrosine as these protons are separated by an accurately known, rigidly fixed distance (r_{HH} = 2.5 Å). Based on this reference build-up rate, distances of 3.1, 3.0, and 3.8 Å were derived for the H_a–H_b, H_a–H_c, and H_a–H_d pairs of VX, respectively, which resulted in the ensemble-averaged conformation of Figure 11. The folded nature of the conformation is evident in the figure and indicates that the *O*-ethyl group and at least one of the *N*-isopropyl groups of VX are in close proximity to one another for a significant length of time when VX is present in aqueous solutions at dilute concentrations.

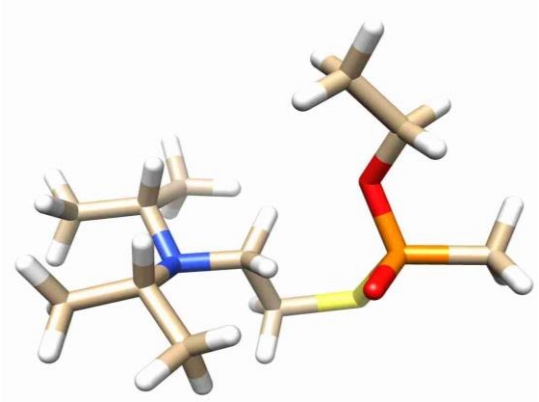

Figure 11. Ensemble-averaged conformation for VX in aqueous solution. Carbon atoms are tan, hydrogen atoms (protons) are white, oxygen atoms are red, phosphorus atoms are orange, sulfur atoms are yellow, and nitrogen atoms are blue.

8. CONCLUSIONS

The conformational flexibility of nerve agents in solution and the selection of a single conformation upon AChE binding have never been investigated in detail. To evaluate these processes, transient NOE build-up curves for nerve agents in solution, together with other NOE data for the AChE-bound agent, will be measured to determine the conformational changes induced upon the nerve agent–AChE binding. The solution conformations of the nerve agents, inferred from measuring build-up curves and other NMR data, will be used along with molecular modeling to examine the induced conformational changes and the accompanying changes in entropy, enthalpy, and free energy for the nerve agent. Initial investigation into the aqueous solution behavior of VX revealed that the *O*-ethyl group and at least one of the *N*-isopropyl groups of the nerve agent molecule are in close proximity to one another for a significant length of time, resulting in a folded, rather than extended, ensemble-averaged conformation.

Blank

LITERATURE CITED

Amit, A.G.; Mariuzza, R.A.; Phillips, S.E.V.; Poljak, R.J. Three-Dimensional Structure of an Antigen-Antibody Complex at 2.8 Å Resolution. *Science* **1986,** *23*, 747–753.

Bryngelson, J.D.; Onuchic, J.N.; Socci, N.D.; Wolynes, P.G. Funnels, Pathways, and the Energy Landscape of Protein Folding: A Synthesis. *Proteins* **1995,** *21*, 167–195.

Cavalli, A.; Bottegoni, G.; Raco, C.; De Vivo, M.; Recanatini, M. A Computational Study of the Binding of Propidium to the Peripheral Anionic Site of Human Acetylcholinesterase. *J. Med. Chem.* **2004,** *47*, 3991–3999.

Enyedy, I.J.; Kovach, I.M.; Bencsura, A. A Molecular Dynamics Study of Active-Site Interactions with Tetracoordinate Transients in Acetylcholinesterase and Its Mutants. *Biochem. J.* **2001,** *353*, 645–653.

Ferrage, F.; Piserchio, A.; Cowburn, D.; Ghose, R. On the Measurement of ^{15}N-{^{1}H} Nuclear Overhauser Effects. *J. Magn. Reson.* **2008,** *192*, 302–313.

Ferreiro, D.U.; Hegler, J.A.; Komives, E.A.; Wolynes, P.G. On the Role of Frustration in the Energy Landscapes of Allosteric Proteins. *Proc. Natl. Acad. Sci. USA* **2011,** *108*, 3499–3503.

Glaudemans, C.P.J; Lerner, L.; Daves, G.D.; Kovác, P.; Venable, R.; Bax, A. Significant Conformational Changes in an Antigenic Carbohydrate Epitope upon Binding to a Monoclonal Antibody. *Biochemistry* **2009,** *29*, 10906–10911.

Lushington, G.H.; Guo, J.-X.; Hurley, M.M. Acetylcholinesterase Reprised: Molecular Modeling with the Whole Toolkit. *Frontiers in Medicinal Chemistry* **2010,** *5*, 423–456.

Radic, Z.; Quinn, D.M.; Vellom C.; Camp, S.; Taylor, P. Allosteric Control of Acetylcholinesterase Catalysis by Fasciculin. *J. Biol. Chem.* **1995,** *270*, 20391–20399.

DISTRIBUTION LIST

The following individuals and organizations were provided with one Adobe portable document format (pdf) electronic version of this report:

U.S. Army Edgewood Chemical
Biological Center (ECBC)
RDCB-DRB-C
ATTN: Henderson, T.
Gardner, W.

Defense Threat Reduction Agency
DTRA-RD-CBD-T
ATTN: Ward, T.
J9-CBS
ATTN: Moore, E.

Department of Homeland Security
DHS-ORD-CSAC
ATTN: Famini, G.

G-3 History Office
U.S. Army RDECOM
ATTN: Smart, J.

ECBC Technical Library
RDCB-DRB-BL
ATTN: Foppiano, S.
Stein, J.

Office of the Chief Counsel
AMSRD-CC
ATTN: Upchurch, V.

Defense Technical Information Center
ATTN: DTIC OA

ECBC Rock Island
RDCB-DES
ATTN: Lee, K.


EDGEWOOD CHEMICAL BIOLOGICAL CENTER
A U.S. Army RDECOM Laboratory